RSC Advances

PAPER

View Article Online
View Journal | View Issue

Cite this: *RSC Adv.*, 2017, **7**, 52321

Heterogeneous hybrid of propyl amino functionalized MCM-41 and 1*H*-1,2,4-triazole for high efficient intermediate temperature proton conductor†

Zhenzhen Wu, Juan Li* and Xian-Ming Zhang*

In this study, we introduced 1*H*-1,2,4-triazole into the ordered nanochannels of propyl amino functioned MCM-41 and then investigated the hybrids' proton conducting performance. A high proton conductivity of 8.34×10^{-3} S cm^{-1} has been obtained at 120 °C, with 5 mol% mole ratio of dangling propyl amino and fully loaded 1*H*-1,2,4-triazole in the silica. The activation energy is 0.55 eV and 1.303 eV in the temperature range below and above 80 °C respectively, indicating that the charge transfer mechanism of the material involved both vehicle and Grotthuss process. The above results showed that loading of 1-*H*-1,2,4-triazole molecules into silica's ordered mesopores is a good strategy for excellent proton conductivity under intermediate temperature.

Received 23rd September 2017
Accepted 31st October 2017

DOI: 10.1039/c7ra10535e

rsc.li/rsc-advances

Introduction

Proton-conducting solids play a pivotal role in proton exchange membrane fuel cells (PEMFCs). Perfluorosulfonic acid polymers, such as Nafion, are the state-of-the-art in proton conductors, which can reach a proton conductivity of 0.1 S cm^{-1} in high relative humidity.[1–3] However, when the operation temperature is above 80 °C, this conductivity always decreases dramatically because of the water loss and nanochannel deformation. This limits PEMFCs' operating temperature to 80 °C. Novel electrolyte membranes with high proton conductivity at temperatures above 120 °C can minimize some of the key problems facing PEMFCs (*i.e.* CO poisoning, water and thermal management) hence reducing the overall cost of the fuel cells and increasing the total energy conversion efficiency. Therefore, developing an intermediate temperature proton conductor independent of water is desperately in need.[4–7]

A classical approach to achieve anhydrous proton conduction is to replace water as the proton carrier with amphoteric N-heterocycles, such as imidazole.[8–12] In these amphoteric molecules, the proton conduction is carried out by the formation and fracture of hydrogen bonds *via* Grotthuss-type mechanism, and thus they can not only donate but also accept protons during the proton transferring process. For better performance, 1-*H*-1,2,4-triazole, with three nitrogen atoms in five membered ring structure, has been used as the non-water proton species because rich nitrogen atoms are beneficial to the effective formation of hydrogen networks inside the silicas' nanochannels and consequently high conductivity. Besides, with the discrete electronic density of triazole ring, 1-*H*-1,2,4-triazole obtains higher electrochemical stability than other N-heterocycles such as imidazole, suitable for fuel cell applications and is able to effective proton conductivity under anhydrous conditions. In the past few decades, heterogeneous hybridization of proton source and porous matrix has proven to be one of the most effective approaches to fabricate anhydrous proton conductors.[13–18] With the confinement effect and large pore volume of porous matrix, high conductivities have been obtained for the porous coordination polymers (PCPs), covalent organic frameworks (COFs), as well as other porous organic polymers.[19–26] Kitagawa and co-workers reported that the imidazole loaded PCPs $[Al(OH)(ndc)]_n$ (ndc = 1,4-naphthalenedicarboxylate) exhibited a proton conductivity of 2.2×10^{-5} S cm^{-1} at 120 °C.[19] In addition, the histamine loaded $[Al(OH)(ndc)]_n$ was also prepared and achieved an anhydrous proton conductivity of 1.7×10^{-3} S cm^{-1} at 150 °C.[21] Jiang *et al.* indicated that mesoporous COF [TPB-DMTP-COF] loaded with imidazole molecules exhibited proton conductivity of 4.37×10^{-3} S cm^{-1} under anhydrous conditions.[25]

However, the poor hydrolysis resistance of the most PCPs and COFs limited the hybrid proton conductors' extensive applicability. From the point of view of atomic economy, it is sensible to utilize some other porous substrate with lower cost and easier preparation method. Periodic mesoporous organosilicas (PMOs), first reported by Asefa *et al.* in 1999, directly forms hybrid organic–inorganic matrices by hydrolysis and condensation reactions with organosilane precursors.[27–29] The

Institute of Crystalline Materials, School of Chemistry & Chemical Engineering, Institute of Molecular Science, Shanxi University, Taiyuan 030006, PR China. E-mail: lj0511@sxu.edu.cn; zhangxm@dns.sxnu.edu.cn

† Electronic supplementary information (ESI) available. See DOI: 10.1039/c7ra10535e

presence of organic units enables PMOs to be functionalized with a large number of desired groups. The PMOs exhibit homogeneous and sometimes even crystalline pore walls. By grafting special acidic groups such as the $-SO_3H$, $-H_2PO_4$ *etc.*[30–37] PMOs have achieved preferable proton conduction. Phosphate functionalized MCM-41 nanospheres showed proton conductivity of 0.015 S cm^{-1} at the relative humidity of 100%, but when the humidity was reduced to 20%, this value quickly dropped to 3.0×10^{-4} S cm^{-1}.

In this study, we used a series of propyl amino functionalized MCM-41 (denoted as MS-PrNH_2 silicas) and 1*H*-1,2,4-triazole to construct the heterogeneous hybrid anhydrous proton conductors. The $-NH_2$ of propyl amino groups and the hydroxyl group on the silica's surface are designed as the Lewis acid sites to immobilize 1*H*-1,2,4-triazole molecules and to form the hydrogen bonding networks for proton conduction. The MS-PrNH_2 silicas offer two advantages compared to other porous matrices. Lower cost and more mature industrial preparation of silicas over PCPs and COFs would promote the industrialization of hybrid proton conductors; large pore volume and tunable pore size allow enough storage space for guest molecules, which could effectively improve the hybrid's proton conductivity. More importantly, their ordered pore walls would provide rapid charge transfer routes for protons. By changing the content of propyl amino groups, the pore volume and BET specific surface area as well as the pore size of silicas could change accordingly. Hereafter, the interaction between 1*H*-1,2,4-triazole and silicas' pore wall can be mediated to exhibit different proton conduction behaviours. To the best of our knowledge, there were few kinds of literature reported on the heterogeneous hybrid proton conductors based on silica matrix. Hence, the present study would provide a flexible and simple method for designing and fabricating high-performance intermediate temperature proton conductors.

Experimental

Chemical and materials

1*H*-1,2,4-Triazole, cetyltrimethylammonium chloride (CTAC), tetramethyl orthosilicate (TMOS), 3-(trimethoxysilyl)-1-propanamine were purchased from TCI organic Chemicals. 1*H*-1,2,4-Triazole were purchased from Aladdin Chemistry Co., Ltd. All the solvents were of analytical quality.

Characterizations

Transmission electron microscopy (TEM) characterization was taken with a JEM-2010 transmission electron microscope (operated at 120 kV). Small-angle X-ray powder diffraction analysis was studied by X-ray diffraction (XRD; Rigaku, Ultima IV with D/teX Ultra) analysis using CuKα radiation with a scan speed of 1° min^{-1} ranging from 1° to 10°. Nitrogen sorption isotherms of samples were measured by a Quantachrome Instruments Quadrasorb SII at 77 K and samples were degassed at 150 °C for 5 h in a vacuum before measurements. The Brunauer–Emmett–Teller (BET) surface area was calculated using experimental points at a relative pressure of P/P_0 (0.05–0.12).

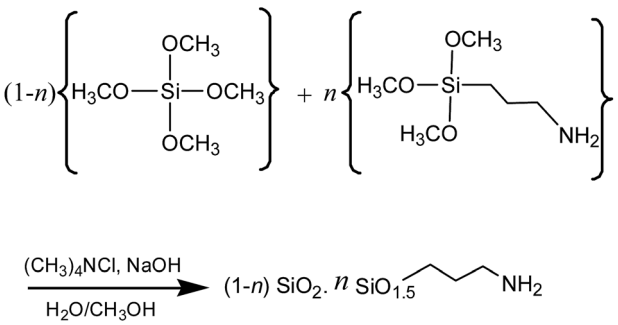

Scheme 1 Synthetic routes of propyl amino functioned MCM-41.

Total pore volume was calculated by the N_2 amount adsorbed at the P/P_0 of 0.99. The pore size distribution was calculated by the DFT method. Proton conductivity measurements were performed on sample pellets using Solartron 1260 analyzer over a frequency range from 1 Hz to 1 MHz and with an amplitude of 100 mV. The sample pellets were tightly connected between two steel electrodes, by means of spring, to ensure good contact between the sample and each electrode. The thickness of sample pellets was measured using a vernier caliper. Measurements were taken under anhydrous conditions and done at thermal equilibrium by holding for 20 min in the whole temperature range. Thermal gravimetric (TGA) experiments were carried out with a Setaram LabsysEvo TG analyzer under a nitrogen atmosphere from 30 °C to 1200 °C with a heating rate of 10 °C min^{-1}. Fourier transform infrared (FTIR) spectra were recorded at room temperature in a KBr matrix on a Nicolet IS 5.

Synthesis of propyl amino-functionalized MCM-41 spheres

Preparation of propyl amino functionalized MCM-41. The propyl amino-functionalized MCM-41 spheres were synthesized according to our previous publication and with some modifications (Scheme 1).[38,39] A typical synthesis method is as the following procedure. 3.52 g CTAC was dissolved in a mixture of 400 mL deionized water, 500 mL methanol, and 2.5 mL NaOH solution (1.0 M), stirring for 30 min at 30 °C. Two solutions of TMOS (2.464 g) in methanol (30 mL) and 3-(trimethoxysilyl)-1-propanamine (0.1451 g) in methanol (30 mL) were prepared. Consequently, they were added dropwise to the above mixture, respectively. After further stirring for 10 h, the resulting solid was isolated by filtration through a filter paper and then washed with water and ethanol, and finally dried at 80 °C for 12 h. To remove the pore-generating template (CTAC), the as-synthesized sample was transferred into an ethanol solution containing ammonium nitrate (0.5 g/150 mL) and stirred for 1 h under reflux. The extraction step was repeated two times to ensure complete removal of CTAC. The template-removed mesoporous silica sphere was washed with deionized water and ethanol for three times and dried at 80 °C overnight under vacuum.

To study the effect of propyl amino groups' amount on final PMOs, the different mole ratio of 3-(trimethoxysilyl)-1-propanamine (5 mol%, 10 mol%, 15 mol% with respect to the

TMOS) were used to synthesize the target silica spheres. Samples denoted as MS-PrNH$_2$-1, MS-PrNH$_2$-2 and MS-PrNH$_2$-3 were obtained by changing the amount of 3-(trimethoxysilyl)-1-propanamine correspondingly during the reaction.

Preparation of 1*H*-1,2,4-triazole loaded silicas. After syntheses MS-PrNH2-1, MS-PrNH2-2 and MS-PrNH2-3 was degassed by heating to 80 °C under reduced pressure for 12 h to remove residual solvent molecules. Then the system was purged with N_2 three times and evacuated at room temperature for 0.5 h. The thermal sublime diffusion method was employed for loading 1*H*-1,2,4-triazole into the pores of silicas. A mixture of silica and 1*H*-1,2,4-triazole was loaded into a Pyrex tube (diameter = 8 mm, length = 130 mm) and this system was sealed under vacuum condition. The Pyrex tube was heated at 120 °C for 48 h to yield the composites, denoted as Tri@MS-PrNH$_2$-1, Tri@MS-PrNH$_2$-2, and Tri@MS-PrNH$_2$-3 respectively, where Tri represents 1*H*-1,2,4-triazole molecules.

Results and discussion

The morphology and microstructure of the silicas before and after loading 1*H*-1,2,4-triazole could be examined directly by transmission electron microscope (TEM). As is shown in Fig. 1(a), the ordered nanochannels with radial pattern could be viewed apparently inside the MS-PrNH$_2$-1. After loading the proton carriers, the surface morphology of Tri@MS-PrNH$_2$-1 is similar to that of MS-PrNH$_2$-1 and the ordered nanochannel was kept well, while it nearly becomes into solid ball as can be clearly seen in Fig. 1(b), indicating the successful loading of the guest molecules into the porous matrix. The TEM images of MS-PrNH$_2$-2, MS-PrNH$_2$-3 and Tri@MS-PrNH$_2$-2, Tri@MS-PrNH$_2$-3 were illustrated in the ESI (Fig. S2 and S3†), both of which showed the similar ordered nanochannel inside the silicas. Further study revealed that proton carriers are accommodate inside the nano-channels of the silicas rather than aggregated on the outer surface. Besides, the nano-channels have not been blocked at the surface, as viewed in the amplified picture of surface morphology of Tri@MS-PrNH$_2$-1. As the content of propyl amino groups increased, we could see that the ordered nanochannel keeps well in MS-PrNH$_2$-2 (Fig. 1(c)) and MS-PrNH$_2$-3 (Fig. 1(e)). However, it is observed in Tri@MS-PrNH$_2$-3 that the central core of the silica sphere is almost hollow (Fig. 1(f)), which shows that the increment of propyl amino groups inside the silica impeded the 1*H*-1,2,4-triazole's accommodation procedure. It can be explained by the above results that the dangling functional groups inside the silica are beneficial to the guest molecules' loading due to their interactions, but the excess of functional groups will lead to the reduction of the porosity. Therefore, only introducing an appropriate amount of propyl amino groups would be good for the introduction of sufficient 1*H*-1,2,4-triazole molecules into silicas.

To investigate the quantity effect of function groups and the loading proton carriers towards the ordered nanochannel of MCM-41 spheres, the small angle XRD patterns of the MS-PrNH$_2$ samples have been measured. As is shown in Fig. 2(a), all of the samples exhibited well-resolved diffraction peak at $2\theta = 2.3°$ ascribed to the (100) reflections, indicating the existence of hexagonal mesophase within the samples. The sharp diffraction peak indicates highly ordered mesoporous structures kept well even when the molar ratio of propyl amino groups was increased to 15 mol%. The intensity of the diffraction peaks of MS-PrNH$_2$-2, MS-PrNH$_2$-3 decreased gradually while becoming broad, which suggests that more propyl amino groups grafted inside the pore wall would reduce the silica's ordered nature to some extent. Furthermore, with the introduction of 1*H*-1,2,4-triazole, the intensity of this diffraction peak decreases obviously and the peak position shifts to high angular displacement, which indicates that 1*H*-1,2,4-triazole molecules have been adsorbed on the silica's internal surface, with an increase of silica's lattice parameter.

The permanent porosity of all the silica samples and their hybrids was evaluated by the N_2 adsorption–desorption isotherm. The BET surface areas, pore volumes and pore sizes are summarized in Table 1. As is shown in Fig. 2(b) and S3,† all the guest free silicas showed a type-IV sorption isotherm, which belongs to the type of a mesoporous material. The total pore volume (pore size) of MS-PrNH$_2$-1, MS-PrNH$_2$-2, MS-PrNH$_2$-3 are 0.7854 cm^3 g^{-1} (3.3 nm), 0.5967 cm^3 g^{-1} (3.1 nm) and 0.4687 cm^3 g^{-1} (3.1 nm) respectively, indicating that more propyl amino groups grafting on the inner space would lead to a significant reduction of MCM-41's total volume and pore size. Similarly, the specific BET surfaces of MS-NH$_2$-1, MS-PrNH$_2$-2, MS-PrNH$_2$-3 reduced gradually from 1004.22 m^2 g^{-1} to

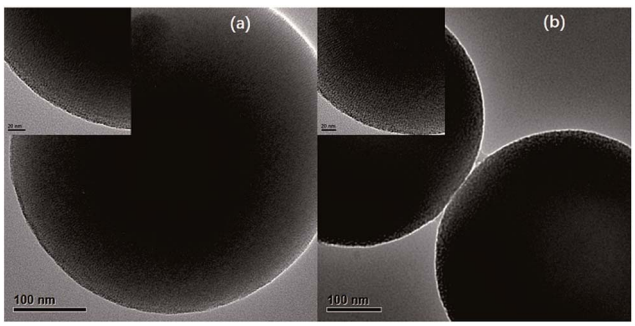

Fig. 1 TEM images of MS-PrNH$_2$-1 (a) and Tri@MS-PrNH$_2$-1 (b).

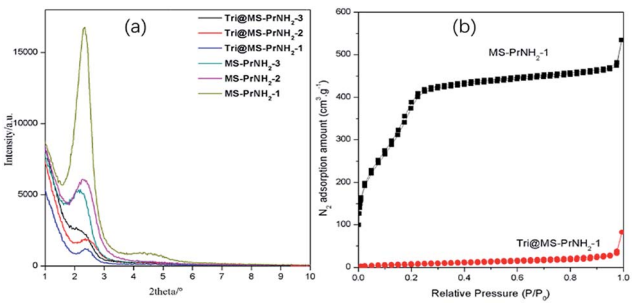

Fig. 2 (a) Small angle powder X-ray diffraction patterns of MS-PrNH$_2$-1, MS-PrNH$_2$-2, MS-PrNH$_2$-3, Tri@MS-PrNH$_2$-1, Tri@MS-PrNH2-2, Tri@MS-PrNH$_2$-3; (b) N_2 adsorption isotherms of MS-PrNH$_2$-1 and Tri@MS-PrNH$_2$-1.

Table 1 The absorption properties of silica

Samples	BET surface area ($m^2\ g^{-1}$)	Pore volume ($cm^3\ g^{-1}$)	Pore size (nm)
MS-PrNH$_2$-1	1004.22	0.7854	3.3
MS-PrNH$_2$-2	804.96	0.5967	3.1
MS-PrNH$_2$-3	541.44	0.4687	3.1
Tri@MS-PrNH$_2$-1	33.82	0.0873	—
Tri@MS-PrNH$_2$-2	18.08	0.0649	—
Tri@MS-PrNH$_2$-3	23.17	0.0759	—

541.44 $m^2\ g^{-1}$, indicating that the silica matrix's loading ability was declining as the increment of grafted propyl amino units. After loading 1*H*-1,2,4-triazole, the total volumes of Tri@MS-PrNH$_2$-1, Tri@MS-PrNH$_2$-2 and Tri@MS-PrNH$_2$-3 were sharply reduced to 0.0873 $cm^3\ g^{-1}$, 0.0649 $cm^3\ g^{-1}$ and 0.0759 $cm^3\ g^{-1}$, respectively, suggesting that the silicas' nanochannels are almost fully occupied by the 1*H*-1,2,4-triazole molecules.

The infrared absorption spectrum was used to explore the possible interaction between 1*H*-1,2,4-triazole and silicas. As is illustrated in Fig. 3a, all the guest free silicas have a strong absorption band at 1075 cm^{-1}, which is attributed to the asymmetric stretching vibration of Si–O–Si. The wide absorption peak at 3436 cm^{-1} is assigned to the OH groups without condensation reaction and NH_2 groups. Peaks at 1524 cm^{-1} and 1627 cm^{-1} correspond to the in-plane bending vibration of the primary NH_2 group. After the loading of 1*H*-1,2,4-triazole, the absorption peak at 3436 cm^{-1} disappeared and some new peaks appeared between 2400 cm^{-1} and 3300 cm^{-1}, which underlines the interactions between 1*H*-1,2,4-triazole and NH_2 groups. In addition, the relative intensity ratios of the two absorption peaks at 1524 cm^{-1} and 1627 cm^{-1} changed significantly, that implies C–C and C–N bonding change in 1*H*-1,2,4-triazole. This result indicates that 1*H*-1,2,4-triazole has been successfully introduced into the pores of silica, while amino functionalization is helpful to the interaction between 1*H*-1,2,4-triazole molecules and pore wall.

To probe the properties of the inner-shell electrons, X-ray photoelectron spectroscopy (XPS) was used. High-resolution narrow scan spectra (Fig. 4) were recorded for the N 1s core

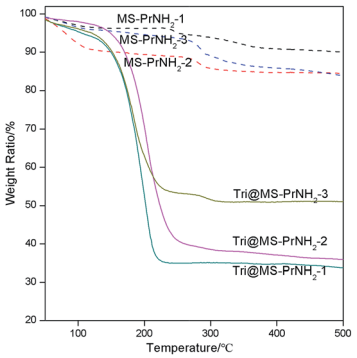

Fig. 4 TGA curves of MS-PrNH$_2$-1, MS-PrNH$_2$-2, MS-PrNH$_2$-3, Tri@MS-PrNH$_2$-1, Tri@MS-PrNH$_2$-2, Tri@MS-PrNH$_2$-3.

levels of MS-PrNH$_2$-1 and Tri@MS-PrNH$_2$-1 for further insight into the compositions and interaction. The XPS study of Tri@MS-PrNH$_2$-1 and MS-PrNH$_2$-1 shows three types of nitrogen atoms: one at 399.7 eV corresponding to the propyl amino nitrogen, the other two at 401.5 eV and 406.7 eV should allude to the protonated secondary amine ($-NH_2^+$). In the spectrum of Tri@MS-PrNH$_2$-1, the relative intensity ratio of $(-NH_2^+)/(-(CH_2)_3NH_2)$ were larger than that of MS-PrNH$_2$-1, that could attribute to the interaction between 1*H*-1,2,4-triazole and grafted amino groups. There is no obvious O 1s binding energy difference between MS-PrNH$_2$-1 and Tri@MS-PrNH$_2$-1 (Fig. S4†), indicating that the main host–guest interaction should not be generated from the hydroxyl groups but from the amino groups.

The loading amount of 1*H*-1,2,4-triazole inside the silicas was checked by thermogravimetric analysis (TGA) measurement (Fig. 5). The first weight loss (<100 °C) of the propyl amino functional MCM-41 can be assigned to the loss of water and residual solvent from the silica spheres. The weight loss at 200 °C can be attributed to the propyl amino groups. All the hybrid samples start obvious weight loss from 150 °C, which presents the removal of 1*H*-1,2,4-triazole. By subtracting the silicas' own weight loss, the weight ratio of 1*H*-1,2,4-triazole in Tri@MS-PrNH$_2$-1, Tri@MS-PrNH$_2$-2, Tri@MS-PrNH$_2$-3 were calculated as 56%, 46% and 29%, respectively. According to

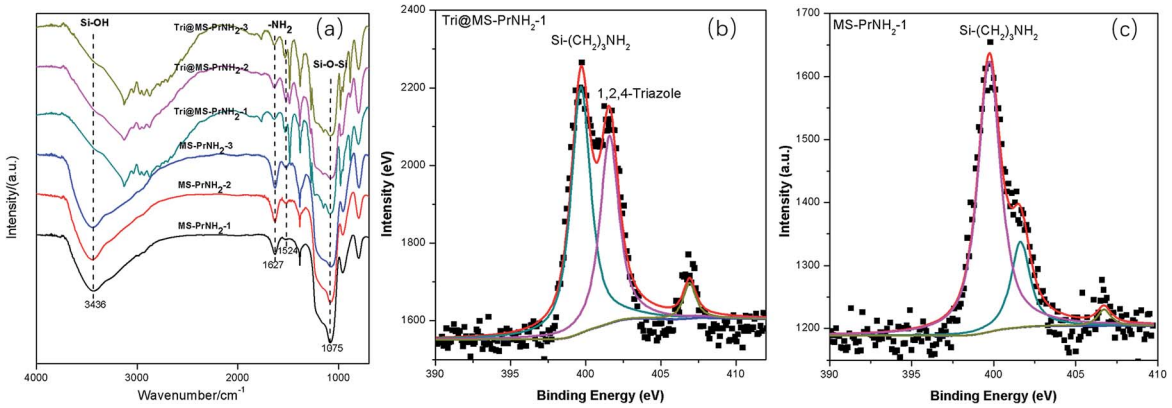

Fig. 3 FTIR spectra of MS-PrNH$_2$-1, MS-PrNH$_2$-2, MS-PrNH$_2$-3 and their composites (a); N 1s X-ray photoelectron spectroscopy of Tri@MS-PrNH$_2$-1 (b) and MS-PrNH$_2$-1 (c).

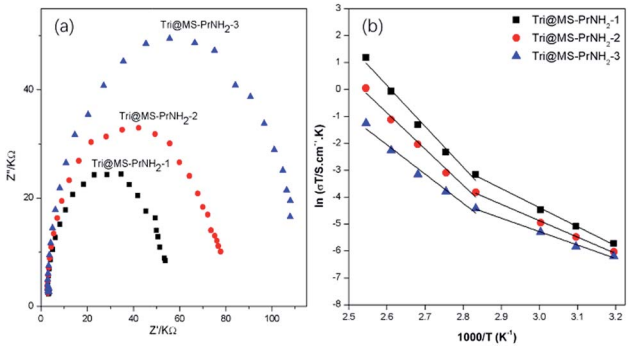

Fig. 5 (a) Nyquist plots (40 °C) and (b) Arrhenius plots of Tri@MS-NH_2-1, Tri@MS-$PrNH_2$-2 and Tri@MS-$PrNH_2$-3.

silicas' total volume and 1*H*-1,2,4-triazole's density, their maximum loading amount should be 50%, 43% and 37%, which largely is consistent with the calculated values.

AC impedance spectroscopy was used to investigate the sample's proton conductivity. It is regarded that the semicircle of all the Nyquist plots in the higher frequency region as bulk resistivity. The conductivity of the samples was calculated from the impedance value using the equation:[40]

$$\sigma = \frac{l}{SR_s}$$

where σ is the conductivity (S cm^{-1}), S is the electrode area (cm^2), l is the measured sample thickness (mm), and R_s, which was extracted directly from the impedance plots, is the bulk resistance of the sample (Ω). The activation energy (E_a) for the material conductivity was estimated from the following equation:

$$\sigma T = \sigma_0 \exp\left(-\frac{E_a}{k_B T}\right)$$

where σ_0 is the pre-exponential factor, k_B is the Boltzmann constant, and T is the sample temperature.

For MS-$PrNH_2$-1, MS-$PrNH_2$-2, MS-$PrNH_2$-3, no semicircles were observed at all, indicating negligible proton conductivity of the idle silicas. The introduction of 1*H*-1,2,4-triazole led to a typical proton conductivity, which was determined from the semicircles in the Nyquist plots (Fig. 5(a)). Tri@MS-$PrNH_2$-1, Tri@MS-$PrNH_2$-2 and Tri@MS-$PrNH_2$-3 displayed proton conductivity of 1.04×10^{-5} S cm^{-1}, 7.66×10^{-6} S cm^{-1} and 6.46×10^{-6} S cm^{-1} at a low temperature of 40 °C. It is notable that although Tri@MS-$PrNH_2$-2 and Tri@MS-$PrNH_2$-3 have more amino groups in their structures, their proton conductivities are lower than Tri@MS-$PrNH_2$-1. This is mainly due to their relatively smaller loading amount of proton carriers that cannot enhance the proton conductivity efficiently. On the other hand, the stronger interaction between 1*H*-1,2,4-triazole and the silica's inner wall might limit 1*H*-1,2,4-triazole's reorientation and hence impede the charge transferring process, which subsequently resulted in lower conductivity.

In order to further demonstrate the effect of the functional groups on the conductivity, we used the pure MCM-41 without propyl amino groups to load the 1*H*-1,2,4-triazole and found that the hybrids didn't exhibit obvious proton conductivity until 90 °C, its highest conductivity obtained at 110 °C is only 10^{-5} S cm^{-1} (Fig. S5†). This demonstrates that the presence of the propyl amino group is indeed beneficial to the improvement of proton conductivity. From the Arrhenius plots (Fig. 5(b)), we could see that all the composites show nonlinear relationships between conductivity and temperatures. Below 80 °C, the E_a of Tri@MS-$PrNH_2$-1, Tri@MS-$PrNH_2$-2, Tri@MS-$PrNH_2$-3 are 0.55 eV, 0.48 eV and 0.40 eV, respectively, which means the proton transfer according to the Grotthuss hopping mechanism. At high temperature above 80 °C, the E_a of these composites increased up to 1.303 eV, 1.159 eV and 0.937 eV, much higher than that in low temperature. It is notable that the activation energy of Tri@MS-$PrNH_2$-1 is relatively higher than Tri@MS-$PrNH_2$-2 and Tri@MS-$PrNH_2$-3. We speculate that this is due to the fact that there are more 1*H*-1,2,4-triazole molecules accommodated in MS-$PrNH_2$-1 and therefore the transmission of protons requires a greater amount of priming.

The proton conductivity of Tri@MS-$PrNH_2$-1 at 120 °C is 8.34×10^{-3} S cm^{-1}, while the corresponding values of Tri@MS-$PrNH_2$-2 and Tri@MS-$PrNH_2$-3 are 2.68×10^{-3} S cm^{-1} and 7.29×10^{-4} S cm^{-1}. Since the concentration of proton species in MS-$PrNH_2$-1 is higher than MS-$PrNH_2$-2 and MS-$PrNH_2$-3, Tri@MS-$PrNH_2$-1 presents a higher proton conductivity. These results show that these hybrid materials have two kinds of proton conduction mechanisms: at temperatures below 80 °C, protons were conducted by the hopping mechanism, while at the higher temperatures, protons would transfer according to the vehicle mechanism. This result is among the best achieved by the hybrid strategy and is comparable to the reported hybrids based on MOFs and POPs as the porous matrix (Table S1 in ESI†).

Conclusions

We have synthesized a series of MCM-41 with different amounts of propyl amino groups incorporated in their inner wall. The pore size and total volume gradually decrease with the improvement of functional groups. Incorporation 1*H*-1,2,4-triazole into silicas' ordered nanochannels on the molecular scale for interaction between the host–guest interaction of NH_2 and 1*H*-1,2,4-triazole has been successfully executed by the evaporation method. With less propyl amino groups decorated in, MS-$PrNH_2$-1 possesses relatively larger interior space than other silicas and hence could accommodate more proton species for a high conductivity of 8.3×10^{-3} S cm^{-1} which is among the best result and can be comparable as hybrid species using MOFs or POPs as porous matrix. With their low cost and mature industrial preparation technology, this kind of propyl amino functional silica material is expected to be utilized as a novel porous matrix for fabricating anhydrous proton conductor. And this study would offer new opportunities for high-performance intermediate proton conductors.

Author contributions

The manuscript was written through contributions of all authors. All authors have given approval to the final version of the manuscript.

Conflicts of interest

There are no conflicts to declare.

Acknowledgements

This work was financially supported by the Sanjin Scholar, the Plan for 10000 Talents in China, and Scientific Research Start-up Funds of Shanxi University (231545004).

Notes and references

1 K. A. Mauritz and R. B. Moore, *Chem. Rev.*, 2004, **104**, 4535–4586.
2 V. A. Deimede and J. K. Kallitsis, *Macromolecules*, 2005, **38**, 9594–9601.
3 F. Zhai, X. Guo, J. Fang and H. Xu, *J. Membr. Sci.*, 2007, **296**, 102–109.
4 G. Titvinidze, K. D. Kreuer, M. Schuster, C. C. de Araujo, J. P. Melchior and W. H. Meyer, *Adv. Funct. Mater.*, 2012, **22**, 4456–4470.
5 J. J. Hernandez, H. Zhang, Y. Chen, M. Rosenthal, M. D. Lingwood, M. Goswami, X. Zhu, M. Moeller, L. A. Madsen and D. A. Ivanov, *Macromolecules*, 2017, **50**, 5392–5401.
6 D. W. Shin, M. D. Guiver and Y. M. Lee, *Chem. Rev.*, 2017, **117**, 4759–4805.
7 Z. Wu, Y. Tang, D. Sun, S. Zhang, Y. Xu, H. Wei and C. Gong, *Polymer*, 2017, **123**, 21–29.
8 J. T. Daycock, G. P. Jones, J. R. N. Evans and J. M. Thomas, *Nature*, 1968, **218**, 672–673.
9 A. Kawada, *J. Chem. Phys.*, 1970, **52**, 3121–3125.
10 K. D. Kreuer, A. Fuchs, M. Ise, M. Spaeth and J. Maier, *Electrochim. Acta*, 1998, **43**, 1281–1288.
11 W. Münch, K. D. Kreuer, W. Silvestri, J. Maier and G. Seifert, *Solid State Ionics*, 2001, **145**, 437–443.
12 S. Li, Z. Zhou, Y. Zhang, M. Liu and W. Li, *Chem. Mater.*, 2005, **17**, 5884–5886.
13 M. Inukai, S. Horike, T. Itakura, R. Shinozaki, N. Ogiwara, D. Umeyama, S. Nagarkar, Y. Nishiyama, M. Malon, A. Hayashi, T. Ohhara, R. Kiyanagi and S. Kitagawa, *J. Am. Chem. Soc.*, 2016, **138**, 8505–8511.
14 H. Yang, X. Sun, S.-X. Liu, Y. Zou, L. Li, J.-L. Liu and X.-M. Ren, *New J. Chem.*, 2016, **40**, 10233–10239.
15 X. Meng, H.-N. Wang, S.-Y. Song and H.-J. Zhang, *Chem. Soc. Rev.*, 2017, **46**, 464–480.
16 H. Wang, Q.-L. Zhu, R. Zou and Q. Xu, *Chem*, 2017, **2**, 52–80.
17 M.-J. Wei, J.-Q. Fu, Y.-D. Wang, J.-Y. Gu, B.-L. Liu, H.-Y. Zang, E.-L. Zhou, K.-Z. Shao and Z.-M. Su, *J. Mater. Chem. A*, 2017, **5**, 1085–1093.
18 Y.-S. Wei, X.-P. Hu, Z. Han, X.-Y. Dong, S.-Q. Zang and T. C. Mak, *J. Am. Chem. Soc.*, 2017, **139**, 3505–3512.
19 S. Bureekaew, S. Horike, M. Higuchi, M. Mizuno, T. Kawamura, D. Tanaka, N. Yanai and S. Kitagawa, *Nat. Mater.*, 2009, **8**, 831–836.
20 J. A. Hurd, R. Vaidhyanathan, V. Thangadurai, C. I. Ratcliffe, I. L. Moudrakovski and G. K. Shimizu, *Nat. Chem.*, 2009, **1**, 705–710.
21 D. Umeyama, S. Horike, M. Inukai, Y. Hijikata and S. Kitagawa, *Angew. Chem.*, 2011, **50**, 11706–11709.
22 S. Horike, D. Umeyama and S. Kitagawa, *Acc. Chem. Res.*, 2013, **46**, 2376–2384.
23 G. Xu, K. Otsubo, T. Yamada, S. Sakaida and H. Kitagawa, *J. Am. Chem. Soc.*, 2013, **135**, 7438–7441.
24 Y. Ye, L. Zhang, Q. Peng, G. E. Wang, Y. Shen, Z. Li, L. Wang, X. Ma, Q. H. Chen, Z. Zhang and S. Xiang, *J. Am. Chem. Soc.*, 2015, **137**, 913–918.
25 H. Xu, S. Tao and D. Jiang, *Nat. Mater.*, 2016, **15**, 722–727.
26 F. Yuan, J. Li, S. Namuangruk, N. Kungwan, J. Guo and C. Wang, *Chem. Mater.*, 2017, **29**, 3971–3979.
27 T. Asefa, M. J. MacLachlan, N. Coombs and G. A. Ozin, *Nature*, 1999, **402**, 867–871.
28 S. Inagaki, S. Guan, Y. Fukushima, T. Ohsuna and O. Terasaki, *J. Am. Chem. Soc.*, 1999, **121**, 9611–9614.
29 B. Hatton, K. Landskron, W. Whitnall, D. Perovic and G. A. Ozin, *Acc. Chem. Res.*, 2005, **38**, 305–312.
30 R. Marschall, I. Bannat, J. Caro and M. Wark, *Microporous Mesoporous Mater.*, 2007, **99**, 190–196.
31 R. Marschall, J. Rathouský and M. Wark, *Chem. Mater.*, 2007, **19**, 6401–6407.
32 M. Wilhelm, M. Jeske, R. Marschall, W. L. Cavalcanti, P. Tölle, C. Köhler, D. Koch, T. Frauenheim, G. Grathwohl, J. Caro and M. Wark, *J. Membr. Sci.*, 2008, **316**, 164–175.
33 Y. G. Jin, S. Z. Qiao, Z. P. Xu, J. C. Diniz da Costa and G. Q. Lu, *J. Phys. Chem. C*, 2009, **113**, 3157–3163.
34 Y. G. Jin, S. Z. Qiao, Z. P. Xu, Z. Yan, Y. Huang, J. C. Diniz da Costa and G. Q. Lu, *J. Mater. Chem.*, 2009, **19**, 2363–2372.
35 M. Sharifi, C. Köhler, P. Tölle, T. Frauenheim and M. Wark, *Small*, 2011, **7**, 1086–1097.
36 S. Fujita, K. Kamazawa, S. Yamamoto, M. Tyagi, T. Araki, J. Sugiyama, N. Hasegawa and M. Kawasumi, *J. Phys. Chem. C*, 2013, **117**, 8727–8736.
37 N. C. Rosero-Navarro, E. M. Domingues, N. Sousa, P. Ferreira and F. M. Figueiredo, *Int. J. Hydrogen Energy*, 2014, **39**, 5338–5349.
38 S. Li, X. Jiao and H. Yang, *Langmuir*, 2013, **29**, 1228–1237.
39 L. Fu, S. Li, Z. Han and H. Liu, *Chem. Commun.*, 2014, **50**, 10045–10048.
40 S. Horike, D. Umeyama, M. Inukai, T. Itakura and S. Kitagawa, *J. Am. Chem. Soc.*, 2012, **134**, 7612–7615.

